

# STAC: Plug-and-Play Spatio-Temporal Aware Cache Compression for Streaming 3D Reconstruction

Runze Wang Yuxuan Song Youcheng Cai\* Ligang Liu  
 University of Science and Technology of China  
<https://stac-3r.github.io/>

## Abstract

Online 3D reconstruction from streaming inputs requires both long-term temporal consistency and efficient memory usage. Although causal VGGT transformers address this challenge through a key-value (KV) cache mechanism, the cache grows linearly with the stream length, creating a major memory bottleneck. Under limited memory budgets, early cache eviction significantly degrades reconstruction quality and temporal consistency. In this work, we observe that attention in causal transformers for 3D reconstruction exhibits intrinsic spatio-temporal sparsity. Based on this insight, we propose *STAC*, a *Spatio-Temporally Aware Cache Compression* framework for streaming 3D reconstruction with large causal transformers. *STAC* consists of three key components: (1) a **Working Temporal Token Caching** mechanism that preserves long-term informative tokens using decayed cumulative attention scores; (2) a **Long-term Spatial Token Caching** scheme that compresses spatially redundant tokens into voxel-aligned representations for memory-efficient storage; and (3) a **Chunk-based Multi-frame Optimization** strategy that jointly processes consecutive frames to improve temporal coherence and GPU efficiency. Extensive experiments show that *STAC* achieves state-of-the-art reconstruction quality while reducing memory consumption by nearly  $10\times$  and accelerating inference by  $4\times$ , substantially improving the scalability of real-time 3D reconstruction in streaming settings.

## 1. Introduction

Reconstructing dense 3D geometry from images remains a fundamental problem in computer vision and graphics. It supports a wide range of applications in virtual and augmented reality [13, 22], robotics [36], and autonomous driving [21]. Traditional reconstruction pipelines such as Structure from Motion (SfM) [24] and Multi-View Stereo (MVS) [12] rely on explicit geometric constraints and op-

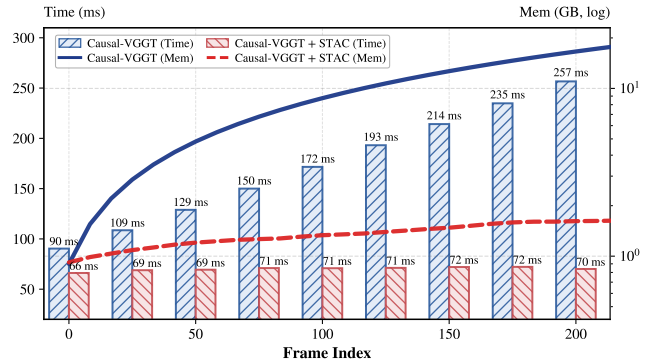


Figure 1. **Runtime-memory scaling in streaming 3D reconstruction.** Bars show per-frame runtime (ms) and lines show KV cache memory (GB, log scale) as the stream grows. Compared with Causal-VGGT, *STAC* reduces KV cache growth and stabilizes per-frame runtime as the stream length increases.

timization to estimate geometry and camera motion. Although these methods are well-established, their high computational cost and limited scalability restrict their applicability in real-time and large-scale scenarios.

Recently, transformer-based architectures are reshaping the field of 3D geometry estimation. VGGT [37] introduces a feed-forward transformer that jointly infers camera parameters, depth maps, point maps, and 3D point tracks from an arbitrary number of input views, achieving state-of-the-art performance without external geometric optimization. Despite this progress, existing methods typically rely on global self-attention or full-sequence processing. In streaming or incremental scenarios, such architectures require all frames to be available beforehand or necessitate recomputation over previous frames, making this batch-processing paradigm unsuitable for online 3D reconstruction and leading to memory and latency inefficiencies. Recent causal variants of VGGT (Causal-VGGT), such as StreamVGGT [49] and SStream3R [14], alleviate these issues by replacing global self-attention with causal self-attention, thereby enabling streaming reconstruction, yet their key-value (KV) cache still grows linearly with sequence length, resulting in substantial memory consump-

\*Corresponding author.

tion and increased latency.

Through analysis of the Causal-VGGT architecture, we observe that its KV cache exhibits structured sparsity along two complementary dimensions: *spatial sparsity*, where tokens correlate with 3D positions and viewpoint changes, and *temporal sparsity*, where certain tokens persistently contribute across frames. However, existing streaming-based approaches treat tokens uniformly, ignoring this structured sparsity, leading to premature eviction of informative tokens and unnecessary caching of transient ones.

To address these limitations, we propose **STAC**, a plug-and-play framework for causal transformer-based 3D reconstruction that exploits structured spatio-temporal sparsity in the KV cache (Fig. 1). Without additional training, STAC performs spatio-temporal KV cache compression for Causal-VGGT, enabling long-term reuse of informative tokens in a memory-efficient manner. Inspired by mechanisms of human memory, STAC maintains two complementary forms of memory. First, **Working Temporal Token Caching** maintains a short-term, high-fidelity working memory that retains recent observations together with a small set of persistent anchor tokens. It combines global reference tokens, a sliding local window, and dynamically selected anchors whose importance is updated via decayed cumulative attention, capturing short-term continuity while preserving globally important cues. Second, **Long-term Spatial Token Caching** maintains a geometry-aware long-term memory. Instead of storing all historical tokens explicitly, it organizes evicted tokens within a voxel grid and progressively merges them into compact voxel-level representations, preserving early-observed geometric information while bounding memory growth over long sequences. Finally, we introduce **Chunk-based Multi-frame Optimization**, which groups a small number of already arrived frames into temporal chunks for joint processing. This allows limited intra-chunk information sharing without accessing future frames, improving both reconstruction consistency and GPU utilization in the streaming setting.

Our main contributions are summarized as follows:

- We identify and analyze the structured spatio-temporal sparsity within causal transformer-based 3D reconstruction, motivating the design of a unified cache compression framework.
- We propose the Spatio-Temporal Aware Cache Compression module, consisting of working temporal caching, long-term spatial caching, and efficient token retrieval to enable compact and consistent memory management.
- We introduce a chunk-based multi-frame strategy that jointly refines consecutive frames, improving temporal coherence and leveraging hardware parallelism.

To the best of our knowledge, STAC provides the first systematic study of *training-free spatio-temporal KV cache compression* for causal transformer-based 3D reconstruction.

Across standard benchmarks, STAC reduces memory usage by nearly  $10\times$  and achieves a  $4\times$  inference speed-up, while delivering reconstruction quality that remains virtually indistinguishable from full Causal-VGGT models.

## 2. Related Work

### 2.1. Feed-Forward 3D Reconstruction

**Traditional methods.** Classical 3D reconstruction pipelines rely on optimization-based, scene-specific processing. Structure-from-Motion (SfM) [24, 29, 41, 42] estimates camera poses via feature extraction and matching [6, 11, 16, 23], triangulation, and bundle adjustment [1, 31], while Multi-View Stereo (MVS) [12, 25, 33] recovers dense geometry. Although accurate and robust, these modular pipelines require sequential optimization, are computationally expensive, and remain sensitive to noise, occlusion, and viewpoint changes.

**Offline approaches.** Recent work has shifted toward feed-forward, end-to-end 3D reconstruction frameworks that bypass explicit geometric optimization. DUST3R [39] models dense reconstruction as direct pointmap regression without requiring camera intrinsics or poses, while MAST3R [15] grounds correspondences in 3D space to enhance generalization. VGGT [37] further unifies multi-view geometry by jointly predicting camera parameters, depth, pointmaps, and feature tracks within a single transformer architecture. Recent variants [9, 26, 45] scale these models to thousands of images and kilometer-scale sequences via parallelization or training-free token merging. Still, they rely on full self-attention over all input tokens, incurring quadratic compute and memory costs and requiring complete re-inference when new frames arrive—limiting their use in streaming scenarios.

**Online/Streaming approaches.** To enable real-time and scalable 3D reconstruction, recent works have explored causal and online transformer formulations. Building on the DUST3R paradigm, prior studies [35, 38, 43] introduce memory mechanisms—such as persistent latent tokens, spatial feature banks, and 3D-aware pointer memories—to support online reconstruction from image streams, but often require architectural specialization or task-specific fine-tuning. More recently, StreamVGGT [49] and Stream3R [14] extend the bidirectional Visual Geometry Grounded Transformer (VGGT) [37] into a causal form (Causal-VGGT). They convert the backbone into a causal transformer and maintain an implicit historical token cache storing keys and values from previous frames to provide temporal context during streaming inference. Benefiting from VGGT’s strong representational capacity, Stream3R in particular achieves state-of-the-art performance on online 3D reconstruction benchmarks. Despite these advances, existing Causal-VGGT methods still suffer from memory and

latency inefficiencies: the KV cache grows linearly with sequence length, leading to high memory consumption and slower inference over long or continuous streams. In contrast, our method introduces a spatio-temporal aware cache compression framework that compresses redundant historical states, maintaining bounded memory usage with minimal impact on reconstruction accuracy.

## 2.2. KV Cache Compression

KV cache compression has been extensively studied in LLMs to alleviate memory and latency bottlenecks under long-context inference. Eviction-based methods such as H2O [48] and StreamLLM [44] retain only a small set of high-importance tokens while discarding the rest, achieving substantial compression with limited quality loss. Merge-based approaches [34, 40] further exploit redundancy in sequential inputs by merging tokens that are about to be evicted into nearby important tokens, thereby reducing information loss under tight memory budgets. In multi-modal and streaming settings, frameworks [10, 18, 46] adopt query- or saliency-driven compression and retrieval, but mainly leverage similarity across neighboring frames or spatial regions. In contrast, our work targets streaming 3D reconstruction and, to our knowledge, is the first to reveal strong spatio-temporal sparsity and local spatial redundancy in the KV cache of large transformer-based 3D models. We explicitly exploit this structure to design a causal, spatio-temporal aware KV compression scheme whose representations remain compact yet temporally coherent, thereby supporting continuous and accurate 3D perception.

## 3. Preliminaries

**VGGT.** The Visual Geometry Grounded Transformer (VGGT) [37] is a unified transformer-based framework for 3D reconstruction from multi-view images. Given a batch of input frames, an image encoder [19] extracts corresponding visual tokens  $F_t$  for each frame. These tokens are jointly aggregated using global self-attention within a multi-view decoder to produce geometry-aware representations:

$$\{G_t\}_{t=1}^T = \text{Decoder}(\text{Global SelfAttn}(\{F_t\}_{t=1}^T)). \quad (1)$$

The geometry-aware tokens  $G_t$  are passed to prediction heads [20] to estimate per-frame camera parameters  $c_t$ , depth maps  $D_t$ , and point maps  $P_t$ :

$$c_t, D_t, P_t = \text{HeadDecoder}(G_t). \quad (2)$$

**Causal-VGGT.** While VGGT operates offline by jointly processing all frames, Causal-VGGT [14, 49] extends the architecture to support streaming inference for 3D reconstruction. It replaces the global self-attention module in the decoder with a causal self-attention mechanism that attends only to past frames, enforcing temporal consistency.

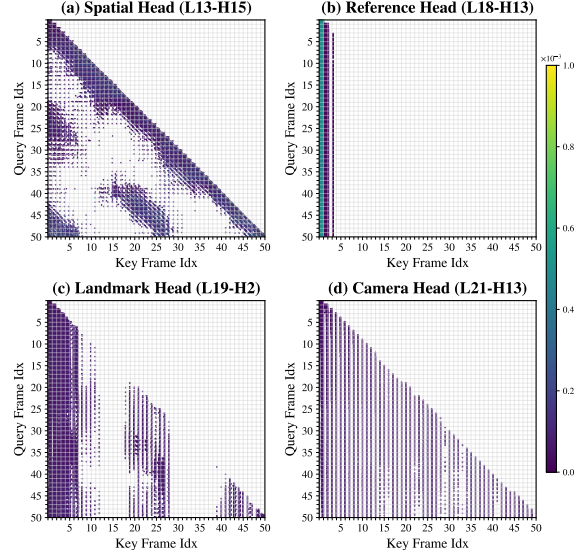


Figure 2. **Spatio-temporal attention sparsity.** Representative attention patterns in the global causal attention map of Causal-VGGT, retaining the top 1024 keys per query for visualization. (a) Spatial attention aligned with camera motion; (b) Persistent focus on first-frame tokens as global references; (c) Temporal anchoring via tokens from semantically stable landmark frames; (d) Long-range attention to camera tokens encoding global context.

To support this causal computation efficiently, Causal-VGGT maintains a key-value (KV) cache that accumulates attention keys and values from previous frames across all decoder layers and attention heads [4, 32]. Specifically, at time step  $t$ , each layer  $\ell$  and head  $h$  stores:

$$\mathcal{M}_t^{\ell,h} = \{\mathbf{m}_\tau^{\ell,h}\}_{\tau=1}^{t-1} = \{\mathbf{k}_\tau^{\ell,h}, \mathbf{v}_\tau^{\ell,h}\}_{\tau=1}^{t-1}, \quad (3)$$

where  $\mathbf{k}_\tau^{\ell,h}$  and  $\mathbf{v}_\tau^{\ell,h}$  are computed via learned projections at each previous step  $\tau$ . These cached representations allow the decoder to incorporate long-term temporal context without reprocessing prior frames.

At each time step, the decoder applies causal self-attention to the current frame’s features  $F_t$ , using the cached keys and values to incorporate temporal context:

$$G_t = \text{Decoder}(\text{Causal SelfAttn}(F_t, \{\mathcal{M}_t^{\ell,h}\}_{\ell,h})). \quad (4)$$

This causal formulation enables efficient streaming inference while maintaining temporal coherence and long-range dependencies learned during training.

## 4. Observation

We begin by analyzing the Causal-VGGT architecture and identify two distinct forms of sparsity within its KV cache: *spatial* and *temporal* sparsity. Visualizations of attention maps (Fig. 2) reveal that different heads specialize in distinct roles—some focus on spatial reasoning, others on tem-

poral consistency. This indicates that Causal-VGGT implicitly organizes spatio-temporal structure, leading to differentiated sparsity patterns in its internal representation.

**Spatial Sparsity.** Certain attention heads exhibit strong spatial sensitivity correlated with camera motion. During loop closures or revisits, these heads consistently focus on visually and spatially adjacent regions across frames (Fig. 2a), indicating that they capture spatial priors useful for cross-view matching and structural consistency. We validate this behavior by analyzing feature similarity and corresponding 3D coordinates, showing that view-dependent tokens often exhibit redundancy in spatially adjacent regions (see Supplementary Material, Sec. A).

**Temporal Sparsity.** Other heads display persistent attention to a small subset of tokens over time, revealing three patterns: (1) *First-frame correlation* – some heads repeatedly attend to the first frame as a global reference (Fig. 2b); (2) *Landmark-frame correlation* – others consistently attend to tokens from semantically stable landmark frames, serving as long-term temporal anchors (Fig. 2c); (3) *Camera-token correlation* – several heads attend to camera tokens, propagating global context (Fig. 2d).

Despite these structured sparsity patterns, prior streaming 3D methods [14, 49] ignore such distinctions and treat all tokens equally. Uniform caching/eviction policies often discard globally important tokens prematurely. This motivates the design of our **Spatio-Temporal Aware Cache Compression (STAC)** module, which explicitly models these sparsity patterns by preserving informative tokens while compactly storing view-dependent ones for future retrieval. This design improves both efficiency and temporal consistency in streaming 3D reconstruction.

## 5. Method

In this section, we introduce **STAC**, a training-free KV cache compression framework for causal transformer-based streaming 3D reconstruction, based on the observations in Sec. 4. As shown in Fig. 3, STAC consists of two complementary components: *Working Temporal Token Caching* (Sec. 5.1), which integrates global reference, local window, and anchor tokens to maintain temporal coherence; and *Long-term Spatial Token Caching* (Sec. 5.2), which organizes evicted tokens in a 3D voxel grid and merges them online for efficient spatial reuse. In addition, *Chunk-based Multi-frame Optimization* (Sec. 5.3) jointly processes consecutive frames to improve both reconstruction accuracy and computational efficiency.

### 5.1. Working Temporal Token Caching

The working temporal cache maintains a compact short-term memory over recent frames while selectively preserving a small set of persistent tokens that remain important over longer time spans. This design exploits the fact that,

in streaming reconstruction, relevant context mainly comes from recent observations and a few globally informative cues. Given a continuous stream of input frames, we construct the working temporal cache at time step  $t$  by integrating three types of tokens:

(1) *Global reference tokens*  $\mathcal{M}^{\text{refer}}$ : the tokens from the first frame  $\mathbf{m}_1$  serve as a global reference, enabling all subsequent frames to be incrementally aligned within a unified coordinate system for stable and consistent reconstruction.

(2) *Local window tokens*  $\mathcal{M}_t^{\text{window}}$ : a sliding temporal window of size  $s$  captures short-term temporal correlations and motion continuity, using tokens from  $\{\mathbf{m}_{t-s}, \dots, \mathbf{m}_{t-1}\}$ .

(3) *Anchor tokens*  $\mathcal{M}_t^{\text{anchor}}$ : persistent informative tokens, including landmark-frame and camera tokens, encoding geometric or camera-related information and dynamically maintained to preserve long-range temporal context.

Accordingly, the working temporal cache at time step  $t$  is defined as:

$$\mathcal{M}_t^{\text{temp}} = \mathcal{M}^{\text{refer}} \cup \mathcal{M}_t^{\text{window}} \cup \mathcal{M}_t^{\text{anchor}}, \quad (5)$$

While  $\mathcal{M}^{\text{refer}}$  is fixed and  $\mathcal{M}_t^{\text{window}}$  is updated by a sliding-window rule,  $\mathcal{M}_t^{\text{anchor}}$  is dynamically maintained under a budget using attention-based importance scores. We next detail the score update and Top- $K$  anchor selection.

**Importance score update.** To track persistent anchor tokens, we maintain a decaying importance score  $s_i$  for each token in the temporal cache  $\mathcal{M}_t^{\text{temp}}$ . At time step  $t$ , the current frame produces query features  $\{q_t^j\}_{j=1}^N$ , and attention weights are computed using scaled dot-product attention:

$$\alpha_t^{j,i} = \text{Softmax}_i \left( q_t^j \cdot \mathbf{k}_t^{\text{all}} / \sqrt{d_h} \right), \quad (6)$$

where the Softmax is taken over the keys  $\mathbf{k}_t^{\text{all}}$  from the working temporal cache  $\mathcal{M}_t^{\text{temp}}$ , the spatial cache  $\mathcal{M}_t^{\text{spat}}$  (Sec. 5.2), and the current-frame tokens  $\mathbf{m}_t$ , for each query  $q_t^j$ . Here,  $d_h$  denotes the per-head feature dimension. The importance scores are then updated with exponential decay:

$$s_t^i = \gamma s_{t-1}^i + \sum_{j=1}^N \alpha_t^{j,i}, \quad i \in \mathcal{I}(\mathcal{M}_t^{\text{temp}}), \quad (7)$$

where  $\gamma \in (0, 1)$  is a decay factor and  $\mathcal{I}(\cdot)$  denotes the index set of cached tokens. For newly generated tokens in the current frame, we initialize  $s_t^i = \sum_j \alpha_t^{j,i}$ .

**Anchor token selection.** After updating the importance scores, we retain the Top- $K$  most informative tokens as the new anchor tokens:

$$\mathcal{M}_{t+1}^{\text{anchor}} = \text{Top-K}(\{\mathbf{m}_i\}, \{s_i\}), \quad i \in \mathcal{I}(\mathcal{M}_t^{\text{anchor}} \cup \mathbf{m}_{t-s}), \quad (8)$$

where  $\mathbf{m}_{t-s}$  represents the tokens that are about to be discarded from the sliding window. This selective update ensures that only salient and temporally stable features are

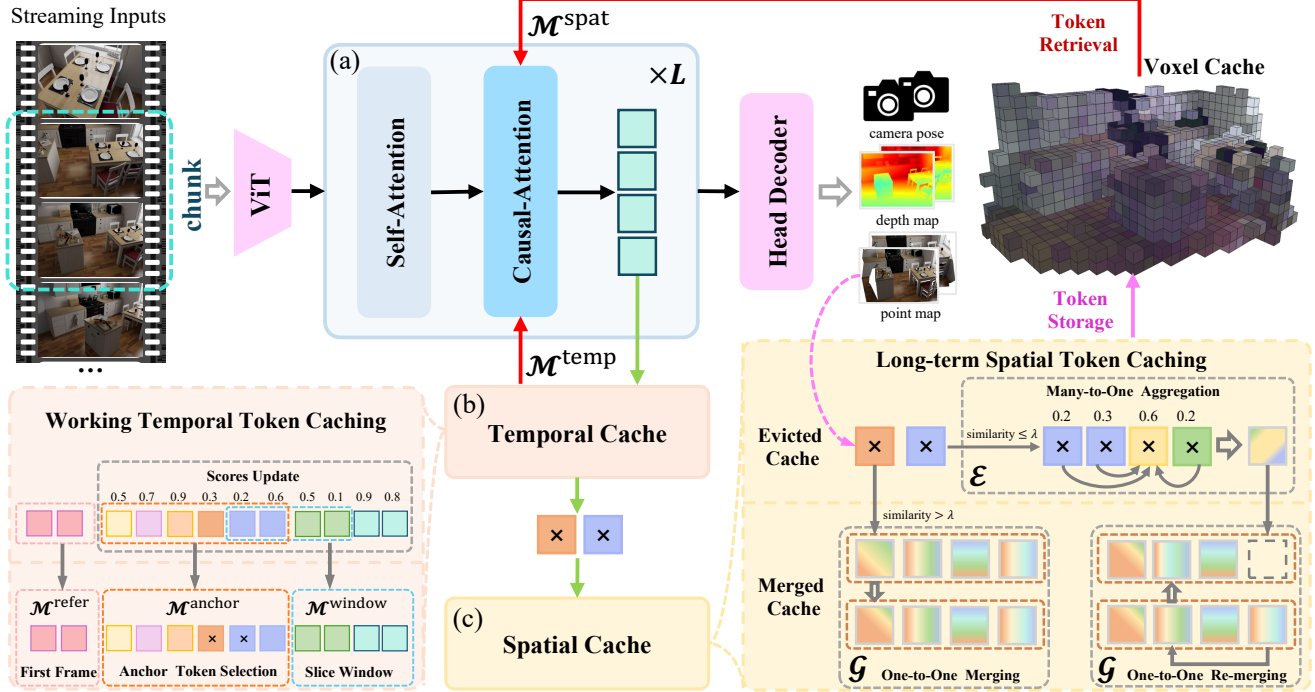


Figure 3. **Overview of STAC.** Our framework reconstructs 3D scenes online using spatio-temporal token caching and chunk-based causal inference. (a) The **Causal-VGGT** module processes ViT-tokenized frames in each chunk using causal attention over the working temporal cache  $\mathcal{M}^{\text{temp}}$  and spatial cache  $\mathcal{M}^{\text{spat}}$  retrieved from a 3D voxel grid. (b) During inference, **Working Temporal Token Caching** updates token scores after each KV cache access, retaining high-scoring anchor tokens  $\mathcal{M}^{\text{anchor}}$  while preserving first-frame reference tokens  $\mathcal{M}^{\text{refer}}$  and sliding-window tokens  $\mathcal{M}^{\text{window}}$ , and evicting the rest. (c) **Long-term Spatial Token Caching** routes evicted tokens with 3D coordinates from the **Head Decoder** to many-to-one aggregation in  $\mathcal{E}$  or one-to-one merging into  $\mathcal{G}$ . When  $\mathcal{G}$  is full, re-merging frees a slot for the incoming merged token, and the updated representations are stored in a 3D voxel grid for future retrieval.

persistently cached, enabling a compact yet expressive temporal memory representation.

## 5.2. Long-term Spatial Token Caching

While the working temporal cache captures short-term coherence, evicting tokens in long sequences discards early spatial evidence and harms later reconstruction. Since retaining all tokens is memory-prohibitive [14, 49], we propose **Long-term Spatial Token Caching**, which exploits 3D spatial redundancy with a voxel-based structure (Sec. 4). Tokens are assigned to voxels by 3D position and compressed independently. Each voxel maintains a dual-cache: a short-term buffer  $\mathcal{E}_u$  for recently evicted tokens and a long-term set  $\mathcal{G}_u$  of merged representatives, preserving feature diversity for long-term spatial reuse.

**Token Merging.** To preserve information from evicted tokens under a fixed memory budget, we cast cache updates as a capacity-constrained online clustering problem. It comprises two complementary operations: *one-to-one merging*, which absorbs an evicted token into its most similar long-term representative to reduce redundancy, and *many-to-one aggregation*, which summarizes buffered tokens into a single representative inserted as a new cluster center to cap-

ture novel observations. Given an evicted token  $m^e = \{k^e, v^e\} \in \mathbb{R}^{2 \times d_h}$  assigned to voxel  $u$ , we update the cache as follows; pseudocode and implementation details are provided in Sec. B of the Supplementary Material.

**Merging with Long-term Tokens.** To eliminate redundancy while reinforcing frequently observed spatial patterns, we match  $m^e$  against representatives  $\hat{m} \in \mathcal{G}_u$  using cosine similarity on key embeddings:

$$\hat{m}^p = \arg \max_{\hat{m} \in \mathcal{G}_u} \cos_k(m^e, \hat{m}), \quad (9)$$

where  $\cos_k(m^e, \hat{m})$  is computed between the key embeddings of  $m^e$  and  $\hat{m}$ . If  $\cos_k(m^e, \hat{m}^p) > \lambda$ , a weighted fusion is performed:

$$\hat{m}^p \leftarrow \frac{Z(\hat{m}^p)\hat{m}^p + \omega(m^e, \hat{m}^p)m^e}{Z(\hat{m}^p) + \omega(m^e, \hat{m}^p)} \quad (10)$$

where  $\omega(\cdot, \cdot) = \exp(\cos_k(\cdot, \cdot))$  following [34]. The cumulative weight is updated as  $Z(\hat{m}^p) \leftarrow Z(\hat{m}^p) + \omega(m^e, \hat{m}^p)$ . Otherwise,  $m^e$  is enqueued into  $\mathcal{E}_u$  to prevent prematurely merging potentially distinctive evidence; this also handles the case where  $\mathcal{G}_u$  is initially empty.

**Aggregation of Evicted Tokens.** To preserve rare yet informative observations that do not satisfy the similarity

threshold, we buffer dissimilar tokens in  $\mathcal{E}_u$  and aggregate them once the buffer reaches capacity:

$$\hat{m} = \frac{\sum_{m \in \mathcal{E}_u} \omega(m, m^q) m}{\sum_{m \in \mathcal{E}_u} \omega(m, m^q)}, \quad (11)$$

where  $m^q$  is the highest-scored (Eq. 7) pivot token in buffer  $\mathcal{E}_u$ , as illustrated in Fig. 3. The cumulative weight is assigned as  $Z(\hat{m}) = \sum_{m \in \mathcal{E}_u} \omega(m, m^q)$ , after which  $\hat{m}$  is inserted into  $\mathcal{G}_u$  as a new representative.

*Re-merging under memory constraints.* Finally, when  $\mathcal{G}_u$  reaches its capacity, we trigger a lightweight compaction step to make room for the incoming merged token. We select the least informative representative  $\hat{m}^l = \arg \min_{\hat{m} \in \mathcal{G}_u} Z(\hat{m})$ , fuse it into its most similar neighbor in  $\mathcal{G}_u \setminus \{\hat{m}^l\}$ , and then discard  $\hat{m}^l$  to free one slot; details are provided in Sec. B.2 of the Supplementary Material.

Our design provides three key advantages: (1) memory efficiency, enabled by voxel-aware compression; (2) long-term consistency, achieved by retaining early-scene information; and (3) feature diversity, preserved via a dual-cache mechanism that maintains heterogeneous representations. Collectively, these properties support scalable and temporally consistent memory for streaming 3D reconstruction.

**Token Retrieval.** To provide spatial context during decoding, we retrieve relevant tokens based on the voxel grid. At each time step  $t$ , the model decodes per-pixel 3D points and voxelizes them to obtain the visible voxel set  $\mathcal{V}^t$ . We then expand it to  $\text{Nbr}(\mathcal{V}^t)$  by k-nearest neighbor (kNN) search over voxel centers to fetch nearby voxels, and retrieve all tokens from the long-term and temporary buffers:

$$\mathcal{M}_t^{\text{pat}} = \{m_t \mid m_t \in \mathcal{G}_u \cup \mathcal{E}_u, u \in \text{Nbr}(\mathcal{V}^t)\}. \quad (12)$$

This localized retrieval ensures that only spatially and semantically relevant tokens are accessed, improving both efficiency and consistency. To compensate for identity loss caused by token merging, we follow [3, 30] and apply a *count-based bias* to correct attention logits. Each merged token carries a count  $n$  and modifies the attention as:

$$q \cdot k / \sqrt{d_h} + \log n, \quad (13)$$

boosting frequently merged tokens during attention (Eq. 6).

### 5.3. Chunk-based Multi-frame Optimization

To improve GPU utilization and reconstruction accuracy during streaming inference, we adopt a *chunk-based multi-frame optimization* strategy. Rather than processing frames strictly one by one, we group a small set of consecutive available frames into temporal chunks and process them jointly. This procedure is *chunk-causal*: at time step  $t$ , each chunk is constructed using only frames available up to  $t$  (i.e., no frames with index  $> t$  are used). Within a chunk, attention is computed bidirectionally across frames,

enabling limited intra-chunk information exchange to enhance local geometric consistency, while the chunk boundary maintains the streaming constraint. In practice, chunk-level execution amortizes kernel-launch overhead and data transfers, thereby substantially improving GPU efficiency compared to frame-by-frame processing.

For memory efficiency, we voxelize cached tokens and map 3D voxel coordinates to contiguous memory indices using Morton codes [7, 17] to preserve spatial locality. We also batch token selection, merging, and retrieval across layers after the forward pass to reduce KV cache overhead.

## 6. Experiments

### 6.1. Implementation Details

We extend Causal-VGGT [14, 49] to support memory-constrained online 3D reconstruction and camera pose estimation. We set the decay factor to  $\gamma = 0.9$ , voxel grid resolution to 0.05, and cosine similarity threshold for token merging to  $\lambda = 0.8$ . Each voxel stores at most  $|\mathcal{G}| = 4$  merged tokens and  $|\mathcal{E}| = 8$  temporarily evicted tokens, with kNN retrieval performed within a  $2 \times$  voxel radius. To enable merge-aware attention, we implement a custom CUDA kernel that computes attention outputs and importance scores. At runtime, the first frame’s KV cache is fully retained. The remaining budget, set to  $8 \times$  the number of frame tokens, is allocated as follows: 50% to the temporal window ( $s = 4$ ), 25% to anchor tokens, and 25% to retrieved merged tokens (with evicted tokens used when insufficient). All KV caches are stored in `float16` to reduce memory consumption. We use chunk size of 4 for multi-frame optimization, and all experiments run on a single 40GB A100 GPU.

**Baselines.** Thanks to its plug and play design, STAC can be seamlessly integrated into Causal-VGGT style causal transformers, including SStream3R [14] and StreamVGGT [49]. We also compare sliding window variants of SStream3R and StreamVGGT, namely SStream3R-W and StreamVGGT-W, which retain the first frame and apply a fixed length temporal window during causal inference, following prior practice [14, 44, 48]. For broader comparison, we evaluate online baselines including Spann3R [35], CUT3R [38], and Point3R [43], which incorporate memory mechanisms but are tightly coupled with architectures in the DUST3R family and typically require fine tuning. In addition, we consider pair based methods such as DUST3R [39], MAST3R [15], and MonST3R [47], which rely on global alignment modules to process streaming inputs.

### 6.2. Evaluation

**3D Reconstruction.** We evaluate STAC on the NRGBD [2] and 7-Scenes [27] datasets, using input images of resolution  $518 \times 392$ . For each sequence, we sample keyframes every 5



Figure 4. Qualitative results on streaming inputs from the 7-scenes and NRGBD datasets.

Table 1. Quantitative results for point cloud reconstruction on the NRGBD and 7 Scenes datasets. Integrating STAC into SStream3R and StreamVGGT substantially improves memory and runtime efficiency while preserving reconstruction quality. W8 denotes a sliding window size of 8. W22 and W26 indicate larger windows for fair total memory, though our method uses less memory at runtime. **Mem**: main values report total memory footprint for comparison; for STAC, this includes the spatial token cache storage, while parentheses show its runtime usage. **FPS**: end-to-end throughput measured over the full reconstruction pipeline, from image input to the final 3D outputs.

Method	Type	NRGBD (stride 5)						7-Scenes (stride 5)						Mem (GB) ↓	FPS ↑
		ACC ↓		Comp ↓		NC ↑		ACC ↓		Comp ↓		NC ↑			
		mean	med	mean	med	mean	med	mean	med	mean	med	mean	med		
DUST3R-GA [39]	Optim	0.619	0.384	0.112	0.028	0.504	0.497	0.406	0.266	0.184	0.055	0.523	0.532	–	<1
MASt3R-GA [15]	Optim	0.599	0.311	0.306	0.096	0.552	0.570	0.459	0.266	0.187	0.040	0.544	0.568	–	<1
MonST3R-GA [47]	Optim	0.528	0.399	0.242	0.098	0.550	0.576	0.328	0.214	0.200	0.031	0.529	0.545	–	<1
CUT3R [38]	Online	0.219	0.142	0.098	0.036	0.612	0.686	0.097	0.050	0.042	0.010	0.585	0.632	0.18	19.79
Spann3R [35]	Online	0.068	0.037	0.020	0.006	0.637	0.733	0.052	0.020	0.019	0.006	0.584	0.628	0.37	57.21
Point3R [43]	Online	0.095	0.047	0.021	0.005	0.668	0.794	0.049	0.023	0.033	0.013	0.595	0.649	1.50	8.34
VGGT [37]	Offline	0.017	0.010	0.012	0.003	0.740	0.881	0.022	0.008	0.024	0.008	0.602	0.658	–	<1
SStream3R [14]	Online	<b>0.053</b>	<b>0.023</b>	<b>0.013</b>	<u>0.005</u>	<b>0.703</b>	<b>0.850</b>	<b>0.044</b>	<b>0.013</b>	<b>0.024</b>	<u>0.007</u>	<b>0.606</b>	<b>0.666</b>	19.75	2.52
SStream3R-W8	Online	0.078	0.036	0.015	<u>0.005</u>	0.687	0.831	0.107	0.037	0.035	0.008	0.587	0.635	<b>0.86</b>	<u>6.19</u>
SStream3R-W22	Online	0.088	0.042	0.019	0.006	0.689	0.839	0.102	<u>0.029</u>	<u>0.029</u>	<b>0.006</b>	0.594	0.647	2.19	5.24
SStream3R-STAC	Online	<u>0.065</u>	<u>0.026</u>	<u>0.014</u>	<b>0.004</b>	<u>0.700</u>	<u>0.847</u>	<u>0.047</u>	<b>0.013</b>	<b>0.024</b>	<b>0.006</b>	<b>0.606</b>	<b>0.666</b>	2.20( <b>0.86</b> )	<b>10.53</b>
StreamVGGT [49]	Online	<u>0.134</u>	<u>0.091</u>	<u>0.059</u>	0.012	<u>0.651</u>	<u>0.772</u>	<b>0.046</b>	<b>0.026</b>	<b>0.027</b>	<b>0.007</b>	<u>0.595</u>	<u>0.648</u>	19.75	2.48
StreamVGGT-W8	Online	0.168	0.101	0.065	0.016	0.647	0.767	0.136	0.058	0.042	<b>0.007</b>	0.584	0.631	<b>0.86</b>	<u>6.10</u>
StreamVGGT-W26	Online	0.174	0.121	0.061	<u>0.011</u>	0.634	0.740	0.117	0.058	0.050	<u>0.010</u>	0.579	0.623	<u>2.57</u>	5.41
StreamVGGT-STAC	Online	<b>0.126</b>	<b>0.081</b>	<b>0.047</b>	<b>0.010</b>	<b>0.682</b>	<b>0.829</b>	<u>0.056</u>	<u>0.030</u>	<u>0.029</u>	<b>0.007</b>	<b>0.596</b>	<b>0.650</b>	2.57( <b>0.86</b> )	<b>10.49</b>

frames, resulting in 200–300 frames per clip, approximating streaming scenarios. Following prior works [35, 39, 43], we report Accuracy (Acc), Completion (Comp), and Normal Consistency (NC) as geometric metrics. For memory and runtime profiling, we measure both the per-frame memory usage and FPS across entire sequences.

Table 1 summarizes the quantitative results; trends in Fig. 1. Integrating STAC into SStream3R and StreamVGGT leads to substantial reductions in memory usage while improving FPS. Meanwhile, reconstruction accuracy remains comparable to, or even exceeds, that of the original models, validating the benefit of explicitly modeling spatio-temporal sparsity within the cache. To further assess the effectiveness of our cache design, we compare STAC with SStream3R-W and StreamVGGT-W. For fairness, we enlarge their sliding-window sizes so that all methods operate under the same memory budget. As shown in Table 1, STAC consistently achieves higher reconstruction accuracy and lower computational overhead under identical memory

constraints, demonstrating the scalability and efficiency of our spatio-temporal cache.

Our method provides superior long-sequence reconstruction quality. While Spann3R [35] and CUT3R [38] rely on implicit or latent memory and thus suffer from long-term drift or forgetting, and Point3R [43] incorporates spatial memory without explicit temporal reasoning, our dual-cache architecture jointly captures long-range temporal cues and structured spatial context. This yields a compact yet expressive memory representation that maintains stability and consistency throughout extended sequences. Quantitative visual comparisons are provided in Fig. 4, further illustrating the advantages of STAC.

**Camera Pose Estimation.** Following [14, 38], we evaluate the task of camera pose estimation on the Sintel [5], TUM Dynamics [28], and ScanNet [8] datasets. We report Absolute Trajectory Error (ATE) and Relative Pose Error (RPE) in both translation and rotation, computed after Sim(3) Umeyama alignment with ground truth trajec-

Table 2. Quantitative camera pose estimation results on the Sintel, TUM Dynamics, and ScanNet datasets.

Method	Type	Sintel			TUM			ScanNet		
		ATE↓	RPE trans↓	RPE rot↓	ATE↓	RPE trans↓	RPE rot↓	ATE↓	RPE trans↓	RPE rot↓
DUST3R-GA [39]	Optim	0.417	0.250	5.796	0.083	0.017	3.567	0.081	0.028	0.784
MASt3R-GA [15]	Optim	0.185	0.060	1.496	0.038	0.012	0.448	0.078	0.020	0.475
MonST3R-GA [47]	Optim	0.111	0.044	0.869	0.098	0.019	0.935	0.077	0.018	0.529
CUT3R [38]	Online	0.213	0.066	0.621	0.046	0.015	0.473	0.099	0.022	0.600
Spann3R [35]	Online	0.329	0.110	4.471	0.056	0.021	0.591	0.096	0.023	0.661
Point3R [43]	Online	0.351	0.128	1.822	0.075	0.029	0.642	0.106	0.035	1.946
VGGT [37]	Offline	0.174	0.056	0.465	0.013	0.010	0.311	0.036	0.015	0.377
SStream3R [14]	Online	<u>0.219</u>	<b>0.065</b>	<b>0.867</b>	<b>0.026</b>	<b>0.013</b>	<b>0.331</b>	<b>0.052</b>	<b>0.021</b>	<b>0.850</b>
SStream3R-W8	Online	0.359	<u>0.081</u>	<u>1.160</u>	0.032	0.015	<u>0.351</u>	0.115	0.040	2.223
SStream3R-STAC	Online	<b>0.198</b>	0.082	1.486	<u>0.030</u>	0.014	<u>0.351</u>	<u>0.053</u>	<u>0.025</u>	<u>0.983</u>
StreamVGGT [49]	Online	<b>0.224</b>	<u>0.092</u>	<b>0.721</b>	<b>0.026</b>	<b>0.012</b>	<b>0.314</b>	<b>0.048</b>	<b>0.019</b>	<b>0.477</b>
StreamVGGT-W8	Online	0.409	<b>0.087</b>	<u>0.918</u>	<u>0.043</u>	0.015	0.331	0.112	0.030	1.459
StreamVGGT-STAC	Online	<u>0.251</u>	0.102	1.341	<b>0.026</b>	<u>0.013</u>	<u>0.326</u>	<u>0.059</u>	<u>0.022</u>	<u>0.531</u>

Table 3. Ablation study of anchor tokens (AC), spatial token caching (SC), count-based bias (CB), and chunk-based optimization (CO), reporting reconstruction metrics, memory, and backbone runtime (excluding the image encoder and head decoders).

Method	Acc ↓	Comp ↓	NC ↑	Mem (GB)	Runtime (ms)
Baseline	0.0776	0.0150	0.6865	0.858	92.56
w/o AC	0.0725	0.0209	0.6991	1.901	61.36
w/o SC	0.0713	0.0199	0.6939	<b>0.572</b>	<b>39.08</b>
w/o CB	0.0666	0.0175	0.6973	2.063	56.08
w/o CO	0.0673	0.0156	0.6948	1.805	138.12
Full	<b>0.0648</b>	<b>0.0142</b>	<b>0.6995</b>	2.210	71.18

tories [47, 49]. As shown in Table 2, SStream3R-STAC and StreamVGGT-STAC achieve competitive pose accuracy compared to SStream3R and StreamVGGT, while operating under a substantially reduced memory budget. The improvements observed on Sintel and TUM further highlight the robustness of our cache design in dynamic scenes, where maintaining long term temporal consistency presents a significant challenge.

### 6.3. Ablation Study

We conduct an ablation study on the NRGBD [2] dataset by removing each key component in isolation, including Anchor Tokens, Spatial Token Caching, Count-based Bias, and Chunk-based Optimization. We use SStream3R-W8 [14] as the baseline. Table 3 summarizes reconstruction quality, memory usage, and runtime performance.

- *Anchor Cache (w/o AC)*. Removing anchor tokens degrades temporal stability due to the loss of persistent geometric and camera-related information.
- *Spatial Cache (w/o SC)*. Disabling spatial caching reduces memory usage and improves speed, but causes a clear drop in reconstruction quality.
- *Count-based Bias (w/o CB)*. Removing CB slightly degrades reconstruction quality, as it fails to compensate for identity loss from token merging.

- *Chunk-based Optimization (w/o CO)*. Without Chunk based Optimization, both quality and runtime degrade, indicating that this component is essential for improving accuracy while maintaining efficient parallelism.

## 7. Conclusion

We present STAC, a training-free framework for streaming 3D reconstruction with a spatio-temporal aware cache compression module. By modeling structured spatial and temporal sparsity in the key-value cache, STAC enables compact memory usage and temporally consistent reconstruction. The proposed working temporal token caching preserves informative tokens via decayed cumulative attention, while long-term spatial token caching compresses redundant features into voxel-based representations for efficient reuse. The chunk-based multi-frame optimization jointly refines consecutive frames, improving temporal coherence and exploiting GPU parallelism for real-time inference. Extensive experiments show that STAC achieves state-of-the-art reconstruction quality with substantially lower memory and computational cost compared to prior streaming transformers. Beyond performance improvements, the framework establishes a unified paradigm for causal 3D perception under constrained memory. Future work explores adaptive cache learning and multimodal extensions to further improve scalability and generalization.

**Limitation.** STAC still has two primary limitations. First, the voxel-based spatial caching depends on a fixed resolution grid. In large or unbounded outdoor scenes, the number of active voxels increases with scene extent, leading to increased memory usage. A practical extension is to offload infrequently accessed tokens to external storage such as the CPU to reduce GPU memory pressure. Second, in highly dynamic environments, fast object motion can introduce inconsistent token representations, which affects the stability of the cache.

## Acknowledgments

This work was supported by the National Natural Science Foundation of China (62025207, U25A20444).

## References

- [1] S. Agarwal, N. Snavely, S. M. Seitz, and R. Szeliski. Bundle adjustment in the large. In *ECCV*, pages 29–42, 2010. 2
- [2] Dejan Azinović, Ricardo Martin-Brualla, Dan B Goldman, Matthias Nießner, and Justus Thies. Neural rgb-d surface reconstruction. In *Proceedings of the IEEE/CVF Conference on Computer Vision and Pattern Recognition*, pages 6290–6301, 2022. 6, 8
- [3] Daniel Bolya, Cheng-Yang Fu, Xiaoliang Dai, Peizhao Zhang, Christoph Feichtenhofer, and Judy Hoffman. Token merging: Your vit but faster. *arXiv preprint arXiv:2210.09461*, 2022. 6
- [4] Tom Brown, Benjamin Mann, Nick Ryder, Melanie Subbiah, Jared D Kaplan, Prafulla Dhariwal, Arvind Neelakantan, Pranav Shyam, Girish Sastry, Amanda Askell, et al. Language models are few-shot learners. *Advances in neural information processing systems*, 33:1877–1901, 2020. 3
- [5] Daniel J Butler, Jonas Wulff, Garrett B Stanley, and Michael J Black. A naturalistic open source movie for optical flow evaluation. In *European Conference on Computer Vision*, pages 611–625, 2012. 7
- [6] Hongkai Chen, Zixin Luo, Jiahui Zhang, Lei Zhou, Xuyang Bai, Zeyu Hu, Chiew-Lan Tai, and Long Quan. Learning to match features with seeded graph matching network. In *Proceedings of the IEEE/CVF International Conference on Computer Vision*, pages 6301–6310, 2021. 2
- [7] Michael Connor and Piyush Kumar. Fast construction of k-nearest neighbor graphs for point clouds. *IEEE Transactions on Visualization and Computer Graphics*, 16(4):599–608, 2010. 6
- [8] Angela Dai, Angel X Chang, Manolis Savva, Maciej Halber, Thomas Funkhouser, and Matthias Nießner. Scannet: Richly-annotated 3d reconstructions of indoor scenes. In *Proceedings of the IEEE Conference on Computer Vision and Pattern Recognition*, pages 5828–5839, 2017. 7
- [9] Kai Deng, Zexin Ti, Jiawei Xu, Jian Yang, and Jin Xie. Vggt-long: Chunk it, loop it, align it—pushing vggt’s limits on kilometer-scale long rgb sequences. *arXiv preprint arXiv:2507.16443*, 2025. 2
- [10] Shangzhe Di, Zhelun Yu, Guanghao Zhang, Haoyuan Li, Tao Zhong, Hao Cheng, Bolin Li, Wanggui He, Fangxun Shu, and Hao Jiang. Streaming video question-answering with in-context video kv-cache retrieval. *arXiv preprint arXiv:2503.00540*, 2025. 3
- [11] Mihai Dusmanu, Ignacio Rocco, Tomas Pajdla, Marc Pollefeys, Josef Sivic, Akihiko Torii, and Torsten Sattler. D2-net: A trainable cnn for joint description and detection of local features. In *Proceedings of the IEEE/CVF Conference on Computer Vision and Pattern Recognition*, pages 8092–8101, 2019. 2
- [12] Yasutaka Furukawa, Carlos Hernández, et al. Multi-view stereo: A tutorial. *Foundations and trends® in Computer Graphics and Vision*, 9(1-2):1–148, 2015. 1, 2
- [13] Ying Jiang, Chang Yu, Tianyi Xie, Xuan Li, Yutao Feng, Huamin Wang, Minchen Li, Henry Lau, Feng Gao, Yin Yang, et al. Vr-gs: A physical dynamics-aware interactive gaussian splatting system in virtual reality. In *ACM SIGGRAPH 2024 Conference Papers*, pages 1–1, 2024. 1
- [14] Yushi Lan, Yihang Luo, Fangzhou Hong, Shangchen Zhou, Honghua Chen, Zhaoyang Lyu, Shuai Yang, Bo Dai, Chen Change Loy, and Xingang Pan. Stream3r: Scalable sequential 3d reconstruction with causal transformer. *arXiv preprint arXiv:2508.10893*, 2025. 1, 2, 3, 4, 5, 6, 7, 8
- [15] Vincent Leroy, Yohann Cabon, and Jérôme Revaud. Grounding image matching in 3d with mast3r. In *European conference on computer vision*, pages 71–91. Springer, 2024. 2, 6, 7, 8
- [16] David G Lowe. Distinctive image features from scale-invariant keypoints. *International Journal of Computer Vision*, 60(2):91–110, 2004. 2
- [17] Guy M Morton. *A computer oriented geodetic data base and a new technique in file sequencing*. International Business Machines Company, 1966. 6
- [18] Zhenyu Ning, Guangda Liu, Qihao Jin, Wenchao Ding, Minyi Guo, and Jieru Zhao. LiveVlm: Efficient online video understanding via streaming-oriented kv cache and retrieval. *arXiv preprint arXiv:2505.15269*, 2025. 3
- [19] Maxime Oquab, Timothée Darcet, Théo Moutakanni, Huy Vo, Marc Szafraniec, Vasil Khalidov, Pierre Fernandez, Daniel Haziza, Francisco Massa, Alaaeldin El-Nouby, et al. Dinov2: Learning robust visual features without supervision. *arXiv preprint arXiv:2304.07193*, 2023. 3
- [20] René Ranftl, Alexey Bochkovskiy, and Vladlen Koltun. Vision transformers for dense prediction. In *Proceedings of the IEEE/CVF International Conference on Computer Vision*, pages 12179–12188, 2021. 3
- [21] Mohamed Reda, Ahmed Onsy, Amira Y Haikal, and Ali Ghanbari. Path planning algorithms in the autonomous driving system: A comprehensive review. *Robotics and Autonomous Systems*, 174:104630, 2024. 1
- [22] Asmaa Sakr and Tariq Abdullah. Virtual, augmented reality and learning analytics impact on learners, and educators: A systematic review. *Education and Information Technologies*, 29(15):19913–19962, 2024. 1
- [23] Paul-Edouard Sarlin, Daniel DeTone, Tomasz Malisiewicz, and Andrew Rabinovich. SuperGlue: Learning feature matching with graph neural networks. In *Proceedings of the IEEE/CVF Conference on Computer Vision and Pattern Recognition*, pages 4938–4947, 2020. 2
- [24] Johannes L Schonberger and Jan-Michael Frahm. Structure-from-motion revisited. In *Proceedings of the IEEE Conference on Computer Vision and Pattern Recognition*, pages 4104–4113, 2016. 1, 2
- [25] Johannes L Schönberger, Enliang Zheng, Jan-Michael Frahm, and Marc Pollefeys. Pixelwise view selection for unstructured multi-view stereo. In *European Conference on Computer Vision*, pages 501–518, 2016. 2

- [26] You Shen, Zhipeng Zhang, Yansong Qu, and Liujuan Cao. Fastvsgt: Training-free acceleration of visual geometry transformer. *arXiv preprint arXiv:2509.02560*, 2025. 2
- [27] Jamie Shotton, Ben Glocker, Christopher Zach, Shahram Izadi, Antonio Criminisi, and Andrew Fitzgibbon. Scene coordinate regression forests for camera relocalization in rgb-d images. In *Proceedings of the IEEE Conference on Computer Vision and Pattern Recognition*, pages 2930–2937, 2013. 6
- [28] Jürgen Sturm, Nikolas Engelhard, Felix Endres, Wolfram Burgard, and Daniel Cremers. A benchmark for the evaluation of rgb-d slam systems. In *2012 IEEE/RSJ International Conference on Intelligent Robots and Systems*, pages 573–580. IEEE, 2012. 7
- [29] Chris Sweeney, Torsten Sattler, Tobias Hollerer, Matthew Turk, and Marc Pollefeys. Optimizing the viewing graph for structure-from-motion. In *Proceedings of the IEEE international conference on computer vision*, pages 801–809, 2015. 2
- [30] Yuxuan Tian, Zihan Wang, Yebo Peng, Aomufei Yuan, Zhiming Wang, Bairen Yi, Xin Liu, Yong Cui, and Tong Yang. Keepkv: Eliminating output perturbation in kv cache compression for efficient llms inference. *arXiv preprint arXiv:2504.09936*, 2025. 6
- [31] Bill Triggs, Philip F McLauchlan, Richard I Hartley, and Andrew W Fitzgibbon. Bundle adjustment—a modern synthesis. In *International Workshop on Vision Algorithms*, pages 298–372, 1999. 2
- [32] Ashish Vaswani, Noam Shazeer, Niki Parmar, Jakob Uszkoreit, Llion Jones, Aidan N Gomez, Łukasz Kaiser, and Illia Polosukhin. Attention is all you need. *Advances in neural information processing systems*, 30, 2017. 3
- [33] Vibhas K Vats, Sripad Joshi, David J Crandall, Md Alimoor Reza, and Soon-heung Jung. Gc-mvsnet: Multi-view, multi-scale, geometrically-consistent multi-view stereo. In *Proceedings of the IEEE/CVF Winter Conference on Applications of Computer Vision*, pages 3242–3252, 2024. 2
- [34] Zhongwei Wan, Xinjian Wu, Yu Zhang, Yi Xin, Chaofan Tao, Zhihong Zhu, Xin Wang, Siqi Luo, Jing Xiong, Longyue Wang, et al. D2o: Dynamic discriminative operations for efficient long-context inference of large language models. *arXiv preprint arXiv:2406.13035*, 2024. 3, 5
- [35] Hengyi Wang and Lourdes Agapito. 3d reconstruction with spatial memory. *arXiv preprint arXiv:2408.16061*, 2024. 2, 6, 7, 8
- [36] Jiaqi Wang, Enze Shi, Huawen Hu, Chong Ma, Yiheng Liu, Xuhui Wang, Yincheng Yao, Xuan Liu, Bao Ge, and Shu Zhang. Large language models for robotics: Opportunities, challenges, and perspectives. *Journal of Automation and Intelligence*, 2024. 1
- [37] Jianyuan Wang, Minghao Chen, Nikita Karaev, Andrea Vedaldi, Christian Rupprecht, and David Novotny. Vgg: Visual geometry grounded transformer. In *Proceedings of the Computer Vision and Pattern Recognition Conference*, pages 5294–5306, 2025. 1, 2, 3, 7, 8
- [38] Qianqian Wang, Yifei Zhang, Aleksander Holynski, Alexei A Efros, and Angjoo Kanazawa. Continuous 3d perception model with persistent state. In *Proceedings of the Computer Vision and Pattern Recognition Conference*, pages 10510–10522, 2025. 2, 6, 7, 8
- [39] Shuzhe Wang, Vincent Leroy, Yohann Cabon, Boris Chidlovskii, and Jerome Revaud. Dust3r: Geometric 3d vision made easy. In *Proceedings of the IEEE/CVF Conference on Computer Vision and Pattern Recognition*, pages 20697–20709, 2024. 2, 6, 7, 8
- [40] Zheng Wang, Boxiao Jin, Zhongzhi Yu, and Minjia Zhang. Model tells you where to merge: Adaptive kv cache merging for llms on long-context tasks. *arXiv preprint arXiv:2407.08454*, 2024. 3
- [41] Kyle Wilson and Noah Snavely. Robust global translations with 1dsfm. In *European Conference on Computer Vision*, pages 61–75, 2014. 2
- [42] Changchang Wu. Towards linear-time incremental structure from motion. In *2013 International Conference on 3D Vision-3DV 2013*, pages 127–134. IEEE, 2013. 2
- [43] Yuqi Wu, Wenzhao Zheng, Jie Zhou, and Jiwen Lu. Point3r: Streaming 3d reconstruction with explicit spatial pointer memory. *arXiv preprint arXiv:2507.02863*, 2025. 2, 6, 7, 8
- [44] Guangxuan Xiao, Yuandong Tian, Beidi Chen, Song Han, and Mike Lewis. Efficient streaming language models with attention sinks. *arXiv preprint arXiv:2309.17453*, 2023. 3, 6
- [45] Jianing Yang, Alexander Sax, Kevin J Liang, Mikael Henaff, Hao Tang, Ang Cao, Joyce Chai, Franziska Meier, and Matt Feiszli. Fast3r: Towards 3d reconstruction of 1000+ images in one forward pass. In *Proceedings of the Computer Vision and Pattern Recognition Conference*, pages 21924–21935, 2025. 2
- [46] Yanlai Yang, Zhuokai Zhao, Satya Narayan Shukla, Aashu Singh, Shlok Kumar Mishra, Lizhu Zhang, and Mengye Ren. Streammem: Query-agnostic kv cache memory for streaming video understanding. *arXiv preprint arXiv:2508.15717*, 2025. 3
- [47] Junyi Zhang, Charles Herrmann, Junhwa Hur, Varun Jampani, Trevor Darrell, Forrester Cole, Deqing Sun, and Ming-Hsuan Yang. Monst3r: A simple approach for estimating geometry in the presence of motion. *arXiv preprint arXiv:2410.03825*, 2024. 6, 7, 8
- [48] Zhenyu Zhang, Ying Sheng, Tianyi Zhou, Tianlong Chen, Lianmin Zheng, Ruisi Cai, Zhao Song, Yuandong Tian, Christopher Ré, Clark Barrett, et al. H2o: Heavy-hitter oracle for efficient generative inference of large language models. *Advances in Neural Information Processing Systems*, 36: 34661–34710, 2023. 3, 6
- [49] Dong Zhuo, Wenzhao Zheng, Jiahe Guo, Yuqi Wu, Jie Zhou, and Jiwen Lu. Streaming 4d visual geometry transformer. *arXiv preprint arXiv:2507.11539*, 2025. 1, 2, 3, 4, 5, 6, 7, 8